INFLUENCE OF MULTIPLE FACTORS ON CALCINED COAL KAOLIN AND NUMERICAL SIMULATION OF ROTARY KILN

Jiale WANG[1], Hongtao KAO[1*]

[1]College of Materials Science and Engineering, Nanjing Tech University, Nanjing 211816, China

[*] Corresponding author: Prof. Hongtao Kao, E-mail: kaoht@163.com

Coal kaolin, as an important industrial raw material, is used in the production of artificial Molochite sand whose application is of great potential for high-end castings due to its ability to significantly reduce the cost of mineral sand and improve the quality of sand mold. In this paper, the key factors in the calcination of coal kaolin were systematically analyzed with a three-factor, four-level orthogonal test, and the test factors were rotary kiln temperature, particle size, and residence time of materials. The optimal calcination parameters determined by range analysis were a temperature of 1500℃ coal kaolin, a particle size of 4mm-8mm, and residence time of 1.5 hours. Analysis of variance showed that temperature had the most significant effect on the calcination effect, followed by coal kaolin particle size. In contrast, the effect of residence time of materials was relatively small. The test showed that the basic needs of producing 60% mullite, the standard percentage, could be met at 1100℃. In order to verify the required coal feed and temperature distribution in the actual rotary kiln, a rotary kiln model was established by numerical simulation technology to simulate the actual conditions. The results showed that the rotary kiln has an average temperature of 1159℃ and a maximum temperature of 1428℃ when the coal consumption is 1.5 kg/s, which meets the temperature requirements for 60% mullite.

Key words*: Orthogonal test; Coal kaolin; Rotary kiln; Temperature; Numerical simulation*

1. Introduction

A significant amount of coal kaolin will be produced in the massive exploitation of coal, accounting for about 10%-15% of the total amount of coal exploited. Coal kaolin is an important industrial raw material with a wide range of applications in paper-making, rubber, plastics, cement, and other industrial fields. It is also used as a natural cleaner for environmental pollutants, achieving the purpose of cleaning with ion exchange or adsorption [1]. Traditionally, coal kaolin is often utilized as a filler in the paper-making and ceramics industries. However, after a series of operations, such as surface modification, it performs better than raw ore. In addition, a representative production process has been established. The purpose of waste utilization can be achieved through the recycling of coal kaolin.

Coal kaolin, as a solid waste in coal mining, can cause serious pollution problems to soil, air, and water resources, making its recycling a key issue [2]. However, Mullite, coal kaolin's main crystallization product after high-temperature calcination, demonstrates good thermal stability, low dielectric loss, and excellent mechanical properties [3]. Therefore, the production of Molochite sand has

become a new direction of coal kaolin utilization. Mullite is the only stable crystalline compound at room temperature and pressure, and its chemical composition ranges from $Al_2O_3/SiO_2 = 3/2$ to $Al_2O_3/SiO_2 = 2/1$. Given the production requirements for high-end casting parts, high-priced mineral sand resources such as chromite sand and forsterite sand are too challenging to be used in large quantities. In this case, artificial Molochite sand emerges as a solution to problems caused by precision casting sand in production. Mullite sand is widely used in the precision casting industry as a shell-making material for investment casting. The ideal chemical formula of coal kaolin is $Al_2O_3 \cdot 2SiO_2 \cdot 2H_2O$, and the following chemical reactions (1-3) will occur in high-temperature calcination. Reaction (1) is the dehydrogenation of coal kaolin to produce metakaolin; reaction (2) is the formation of Al-Si spinel; and reaction (3) is the formation of mullite [4].

$$Al_2O_3 \cdot 2SiO_2 \cdot 2H_2O \rightarrow Al_2O_3 \cdot 2SiO_2 + 2H_2O \quad (1)$$

$$2(Al_2O_3 \cdot 2SiO_2) \rightarrow 2Al_2O_3 \cdot 3SiO_2 + SiO_2 \quad (2)$$

$$3(2Al_2O_3 \cdot 3SiO_2) \rightarrow 2(3Al_2O_3 \cdot 2SiO_2) + 5SiO_2 \quad (3)$$

Ondro *et al.* [5] performed the kinetic analysis of mullite and cristobalite in kaolin, and measured the apparent activation energies of cristobalite and mullite, which were (565±38) kj/mol and (726±9) kj/mol, respectively, using Kissinger's method. Yuan *et al.* [6] analyzed the calcined samples of coal kaolin with the addition of carbonaceous substances using X-ray diffraction and other techniques. The relative decomposition rates were 84.22%, 85.69%, and 88.73% for addition contents of 2%, 4%, and 6%, respectively. Chargui *et al.* [7] investigated the material transformation of kaolin-aluminum dross mixtures during the heating process, and the mullitization of the mixtures was almost complete at temperatures up to 1500℃. The metakaolin reacted to produce primary mullite, and the aluminum dross reacted with the excess silica in kaolin to produce secondary mullite. Chen, *et al.* [8] investigated the crystal transition of kaolin into mullite as a reaction system, focusing on mineral morphology changes 450-1600 ℃, and found that mullite with a high texture could be produced at temperatures above 1500℃.

Rotary kiln is a type of industrial heat exchanger, is widely used in metallurgy, building materials, chemical engineering and other industrial preparation processes. It is mainly responsible for the combustion of fuel, heat exchange of gas and material, calcination of clinker and transportation in industrial applications. The rotary kiln is inclined at an angle of 3.5°-5° to the horizontal plane. The residence time of materials in the rotary kiln is affected by factors such as inclination angle, rotation speed and feed rate [9, 10]. In the related research of rotary kilns, recycling of various wastes is the most significant trend.

Gürtürk *et al.* [11] investigated the use of rotary kilns in gypsum plants by modeling two different rotary kilns using CFD software and analyzing the parameters such as mass fractions of O_2, CO_2, CO, and CH_4, and concluded that there is an excellent potential for improving the energy efficiency of rotary kilns. Ariyaratne *et al.* [12] investigated the fuel feed position and fuel particle size by simulating the combustion of pulverized coal and meat and bone meal (MBM) using CFD software. At the same thermal energy, combustion of MBM produces lower gas temperatures than pulverized coal. For a given fuel, the mass-weighted average particle diameter is negatively correlated with the coke burn-off rate. At the feed position, the feed annulus outperforms the central tube in terms of devolatilization and coke combustion rate. Huang *et al.* [13] investigated the effect of different combustion atmospheres in a rotary kiln using Fluent software and explored the changes in the velocity field, temperature field, and other results by changing the oxygen concentration. The best NO_X emission reduction was achieved when the oxygen concentration reached 27%.

As can be concluded from the above studies, some theoretical systems have been established in existing studies on the transformation of coal kaolin into mullite. However, in the process of calcining coal kaolin on an industrial scale, a variety of working condition factors shall be taken into account, such as particle size of coal kaolin, residence time, and calcination temperature. Researching rotary kilns using Fluent, a computational fluid dynamics (CFD) software, is feasible. Currently, simulation studies based on rotary kilns are limited with respect to the calcination temperature of coal kaolin, so there is still much room for improvement in this field. By altering various parameters, numerical simulation techniques predict the impact on rotary kiln performance under different working conditions. The application of numerical simulation reduces resource consumption. The simulation results can be clearly presented, and the design can be optimized based on these results.

In this paper, a muffle furnace was used to construct the actual environment of the rotary kiln for calcining coal kaolin. Fluent software was used to simulate the actual calcination environment in the rotary kiln. With the calcining kiln of a kaolin company as the research object, the maximum production rate of mullite was obtained with a three-factor, four-level orthogonal test, which investigated kaolin particle size, rotary kiln calcination temperature, and residence time. The relevant distribution of the temperature field and the component field was obtained through numerical simulation analysis, and temperature distribution inside the kiln was analyzed and discussed on the basis of the orthogonal test. The results provided a reference for improving actual operations in the rotary kiln. Also, they provided a practical basis for improving the calcination technology of coal kaolin.

2. Thermal Analysis Test

2.1. Raw Materials

Coal kaolin extracted from the Huaibei coal mine in Anhui Province was selected. The orebody in this mining area is stable, with kaolinite as the primary mineral. It exhibits a high degree of crystallinity and a SiO_2/Al_2O_3 molar ratio close to the theoretical value of 2.0. The coal kaolin was analyzed with X-ray fluorescence. The XRF instrument used was the Panalytical Zetium, which utilized Omnian software for elemental and standardless methods. Its oxide composition is shown in Tab. 1.

The test samples were analyzed with XRD as shown in Fig. 1. The test samples were dominated with coal kaolin with a content of more than 95%.

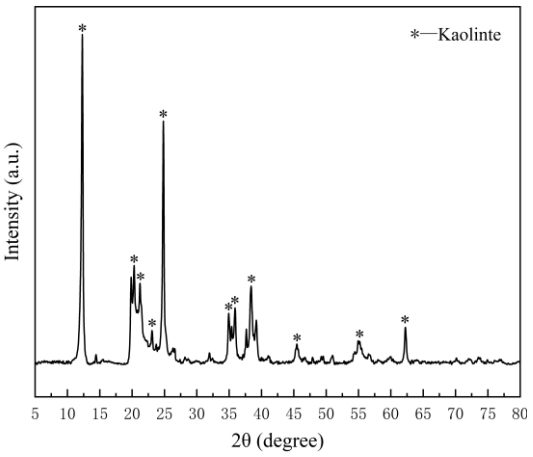

Fig. 1. XRD Pattern of Coal Kaolin

Table 1. Oxide Composition of Coal Kaolin

Name	SiO_2	Al_2O_3	TiO_2	Fe_2O_3	Others
Content (%)	48.2	49.335	0.671	0.939	0.834

2.2. Thermal Analysis

A comprehensive thermal analysis of the coal kaolin was performed with thermogravimetric analysis (TGA) and differential scanning calorimetry (DSC) as shown in Fig. 2. The TG-DSC instrument

used was the TA SDT Q600. The TG standard followed was GB/T 33047.1-2016, and the DSC standard followed was GB/T 19466.2-2004.

The analysis of the TG-DSC chart found that the samples always showed weight loss in the test temperature range; the weight loss of the samples was mainly divided into three phases: 25-500 ℃, 500-700 ℃, and 700-1200 ℃. The weight loss of 25-500 ℃ is mainly caused by the evaporation of free water and the combustion of organic matter contained in the samples. In this phase, the rate of weight loss is low, with an average rate of 0.15%/min, for a weight loss of 3.45%. The weight loss of 500-700 ℃ is mainly caused by the evaporation of constitution water in the samples, and a large amount of weight loss occurs in this phase, with an average rate of 0.94%/min, for a weight loss of 10.01%. The weight loss of 700-1200 ℃ is caused by the transformation of coal kaolin to mullite after dehydration, with a weight loss of 1.17% and an average rate of 0.046%/min. The total weight loss of the three phases is 14.63%.

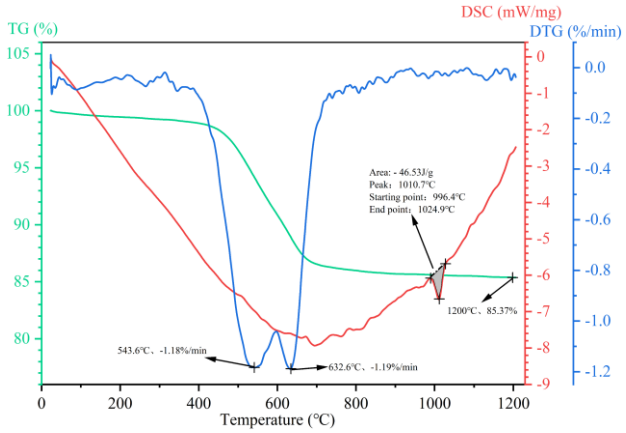

Fig. 2. TG-DSC Chart

3. Orthogonal Test

The selection of factors is crucial for the orthogonal test, because orthogonal analysis will be affected if there is mutual influence between the factors [14]. Three independent factors that do not interfere with each other were selected, namely particle size of coal kaolin (particle size), temperature of the rotary kiln (temperature), and residence time of materials (residence time). At the same time, four levels were selected for each of the three factors. The specific test factor levels are shown in Tab.2.

Table 2. Factor Levels

Factor	Particle size A (mm)	Temperature B (℃)	Residence time C (h)
Level	<2	900	0
	2-4	1100	1
	4-8	1300	1.5
	>10	1500	2

In this paper, a calibrated muffle furnace was used to simulate the internal temperature environment of a rotary kiln, with a temperature error range of ±5°C. The heating rate was controlled by an instrument program, strictly at 10℃/min. Additionally, measurements were retaken at the start of the experiment to ensure accuracy. The calcination process was carried out under an air atmosphere, and in the numerical simulation section of this study, air was also injected into the rotary kiln.

3.1. Orthogonal Test Design

A three-factor four-level orthogonal test was designed. The specific test programs is shown in Tab. 3.

Table 3. Orthogonal Test

Serial No	Particle size A (mm)	Temperature B (℃)	Residence time C (h)
1	<2	900	0
2	<2	1100	1
3	<2	1300	1.5
4	<2	1500	2
5	2-4	900	1
6	2-4	1100	0
7	2-4	1300	2
8	2-4	1500	1.5
9	4-8	900	1.5
10	4-8	1100	2
11	4-8	1300	0
12	4-8	1500	1
13	>10	900	2
14	>10	1100	1.5
15	>10	1300	1
16	>10	1500	0

3.2. Test Results and Analysis

The test results are shown in Fig. 3. By comparing the percentage of mullite of the results from the orthogonal experiment, it is concluded that the samples were best converted (93.4%) when particle size was 4mm-8mm with a 1500°C temperature and 1-hour residence time.

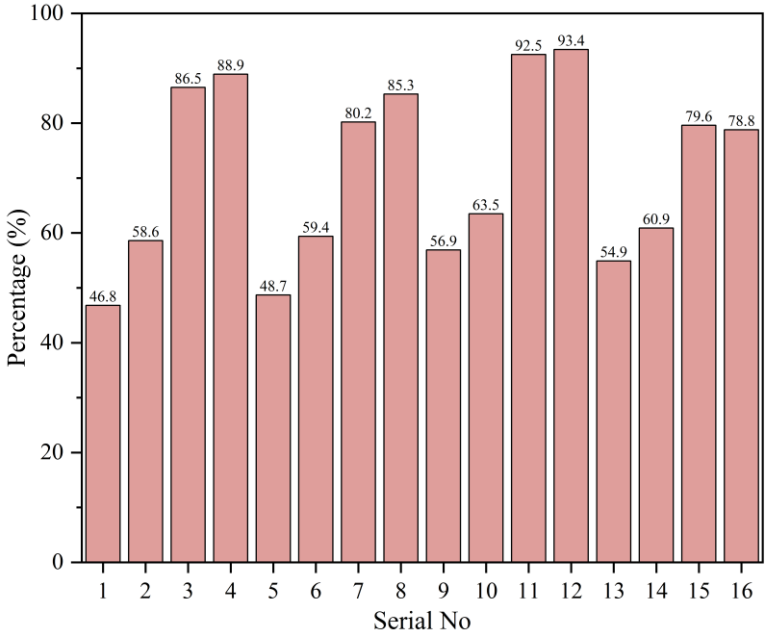

Fig. 3. Orthogonal Test Results

The test results are consistent with the proposed findings. Chargui *et al.* [7] investigated that mullite formation from kaolin is essentially completed at 1500°C. Chen *et al.* [8] found that high-quality mullite can be formed at temperatures above 1500°C.

3.2.1 Range analysis

The results corresponding to different levels in the factors are carried out range calculation. The orthogonal test range analysis is shown in Tab. 4.

Table 4. Range Analysis

Factor		A	B	C
Percentage of mullite	K_1	280.8	207.3	277.5
	K_2	273.6	242.4	280.3
	K_3	306.3	338.8	289.6
	K_4	274.2	346.4	287.5
	k_1	70.2	51.825	69.375
	k_2	68.4	60.6	70.075
	k_3	76.575	84.7	72.4
	k_4	68.55	86.6	71.875
	Range (R)	8.025	34.775	3.025
Factor priority		BAC		
Optimal combination		A3B4C3		

Where K is the sum of the results corresponding to the i level of a specific factor. k is the average value of K. R is the range value.

$$k = \frac{K}{4}, R = k_{max} - k_{min} \quad (4)$$

A more considerable range value indicates that the corresponding factor has a more significant influence on the results. From the range analysis, the range of the three factors of particle size, temperature, and residence time were 8.025, 34.775, and 3.025, respectively. Therefore, the order of influence was temperature, particle size, and residence time. A more considerable K value indicates a better effect at that level. Therefore, the optimal calcination parameters were 4mm-8mm, 1500℃, 1.5h. Range analysis was not in the test scope. A separate test is necessary for this scheme. Upon analysis, the percentage of mullite was 87.6%.

3.2.2 Analysis of variance

The orthogonal test analysis of variance is shown in Tab. 5. Through the comparison of contribution rate, temperature accounts for 94.7%, particle size for 4.6%, and holding time for 0.7%. it can be concluded that temperature is the main factor affecting the percentage of mullite.

Table 5. Analysis of variance

Indicator	source of variance	SS	df	Ms	F	Contribution rate (CR)	Significance
Percentage of mullite	A	177.86	3	59.286	3.359	4.6%	*
	B	3627.5	3	1209.2	68.509	94.7%	**
	C	24.812	3	8.2706	0.4686	0.7%	
	Se	105.9	6	17.65	/		
	Sum	3936.1	15	/	/		

where SS is the sum of squares, df is the degrees of freedom for the factor**,** Ms is the mean square , F is the test statistic, Se is the standard error.

$$df = 4 - 1 = 3, Ms = \frac{SS}{df}, F = \frac{Ms}{Ms_e}, \ CR = \frac{F_i}{\sum F} \tag{5}$$

For the orthogonal analysis, as the rotary kiln environment was constructed with a muffle furnace, the temperature was raised from room temperature to the target temperature at 10℃/min. The samples were removed with high-temperature operating equipment after reaching the target temperature, so the time when the samples were in the furnace was significantly reduced, thus reducing the influence of residence time. In this case, there is a minor significance for the residence time.

3.2.3 XRD analysis of calcined samples

In this paper, charts with corresponding serial No. were selected from Tab.3 at 1300℃ and 1500℃, as shown in Fig. 4 and 5. When the calcination temperature exceeds 1300℃, the diffraction peaks of mullite are obvious in the XRD patterns of Fig. 4 and 5, and the XRD patterns at 1300℃ and 1500℃ all show obvious mullite diffraction peaks.

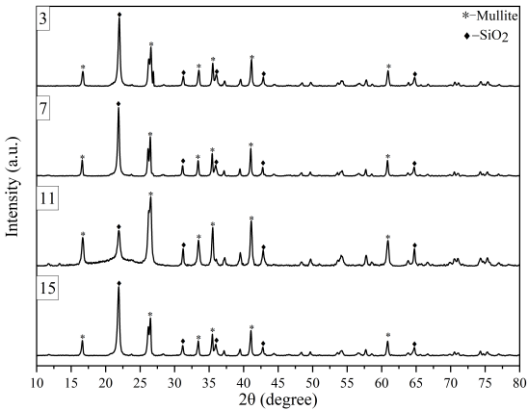

Fig. 4. 1300℃-XRD Diffraction Pattern

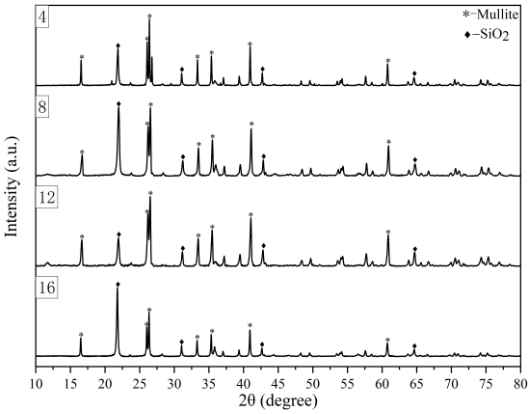

Fig. 5. 1500℃-XRD Diffraction Pattern

4. Numerical Simulation Models and Methods

The calcination temperature shall be 1100℃ in order to meet the production standard for 60% mullite. In the actual production process, however, the temperature in a rotary kiln is much higher than 1100℃. Therefore, this part optimizes the combustion state of the rotary kiln using numerical simulation techniques to seek the optimization scheme for the lowest fuel consumption.

The rotary kiln speed is neglected, and the simulation is performed in a steady state [12, 13]. Through this calculation, using a larger computational load for simulation, the kiln system can achieve equilibrium and maintain stable operation, with all parameter values remaining consistent. In the numerical simulation, the gas introduced into the kiln is air. The operation of the muffle furnace is also conducted under conditions where air is injected. The fluid flow process in the rotary kiln is always limited by the laws of conservation of mass, energy and momentum. The pulverized coal combustion is calculated with a vortex dissipation model. The radiation heat transfer is modeled with the P1 radiation model [15]. The motion of solid particles in the gas phase is modeled with the discrete phase model (DPM) [16].

4.1. Gas-Phase Turbulence Model

Rotary kilns consume a large volume of secondary air and primary air incoming with pulverized coal, but their pipelines for such process have a small cross-sectional area. After the comprehensive consideration, the realizable k-ε model with a wider range of applicability is chosen to simulate the gas-phase turbulent flow [17]. The relevant turbulence energy and dissipation transport equations are as follows:

$$\frac{\partial(\rho k)}{\partial t}+\frac{\partial(\rho k u_i)}{\partial x_i}=\frac{\partial}{\partial x_j}\left[\left(u+\frac{u_l}{\sigma k}\right)\frac{\partial k}{\partial x_j}\right]+G_k+G_b-\rho\varepsilon-Y_M+S_k \tag{6}$$

$$\frac{\partial(\rho\varepsilon)}{\partial t}+\frac{\partial(\rho\varepsilon u_i)}{\partial x_i}=\frac{\partial}{\partial x_j}\left[\left(u+\frac{u_t}{\sigma_\varepsilon}\right)\frac{\partial\varepsilon}{\partial x_j}\right]+\rho C_1 S_\varepsilon-\rho C_2\frac{\varepsilon^2}{k+\sqrt{v\varepsilon}}+ +C_{1\varepsilon}\frac{\varepsilon}{k}C_{3\varepsilon}G_b+S_\varepsilon \tag{7}$$

$$C_1=\max\left[0.43,\frac{\eta}{\eta+5}\right],\eta=\mathrm{S}\frac{k}{\varepsilon},\mathrm{S}=\sqrt{2S_{ij}S_{ij}} \tag{8}$$

Where G_b is the turbulent energy due to buoyancy, G_k is the turbulent energy due to turbulent velocity gradient, Y_M is the over-diffused fluctuation in compressible turbulence, σ_ε and σ_k correspond to the turbulent Prandtl number for equations ε and k, respectively, and S_ε and S_k are custom sources.

4.2. Fuel Combustion Model

In industrial applications, rotary kilns generally employ pulverized coal, natural gas, and a mixture of some alternative fuels (e.g., liquid waste, waste tires, and biomass fuels [18, 19].). After the comprehensive consideration, pulverized coal is used as the fuel in this numerical simulation. The combustion of pulverized coal is divided into two parts, that is, combustion of volatile matter and coke. After the pulverized coal is injected with the burner, the volatile matters are precipitated and burned first, followed by the combustion of residual coke particles. The pyrolysis process of pulverized coal is modeled with the two-step competitive rate model proposed with Kobayashi [20], which has the advantage of high equation accuracy and fast calculation speed. The volatile release rate equation is as follows:

$$\frac{m_v(t)}{m_{p,0}-m_a}=\int_0^t(a_1R_1+a_2R_2)\exp\left(-\int_0^t(R_1+R_2)\,dt\right)dt \tag{9}$$

Where $m_v(t)$ is the mass of volatiles produced with the combustion of pulverized coal during the reaction time, $m_{p,0}$ and m_a are the mass of volatiles in the initial state of pulverized coal and the ash content of volatiles, respectively, and a_1 and a_2 are the low-temperature and high-temperature volatile release rate factors, respectively. R_1 and R_2 are the reaction rate constants.

When the volatiles are released and burned, the residual coke begins to react. The rotary kiln model uses a power/diffusion controlled reaction model with a high fit to the coke [21]. The coke combustion rate is as follow:

$$\frac{dm_p}{dt}=-\pi d_p^2P_{ox}\frac{k_1k_2}{k_1+k_2} \tag{10}$$

Where d_p is the coke particle size, P_{ox} is the partial pressure of oxygen around the coke particles, k_1 is the diffusion factor for oxygen diffusion to the surface of coke particles, and k_2 is the coefficient of reaction kinetics.

4.3. Geometric Model

The rotary kiln required for calcination of coal kaolin in this case is consistent with the actual plant. As shown in Fig. 6, the rotary kiln is divided into three parts, namely outlet, cylinder and inlet, with a total length of 54 m. The outlet pipe diameter is 4.2 m, and the inlet pipe diameter is 4 m.

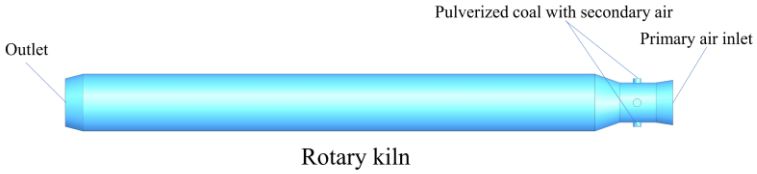

Fig. 6. Structural Diagram of Rotary Kiln

Figure 7 is the grid diagram of the rotary kiln. The model grids are all in a hexahedral structure. And in order to ensure the stable results of the model forms, the grid quantity is controlled at 800,000 orders of magnitude after comprehensive consideration of the computational burden and accuracy, and the total number of grids after partitioning is 884,521. Additionally, grid encryption is carried out in the boundary fields of the inlet and outlet, thereby ensuring correct simulation results.

Fig. 7. Grid Diagram of Rotary Kiln

4.4. Boundary Conditions

The rotary kiln outlet boundary type is “escape”, and the rest of the inlet boundary types are “reflect”. No slip boundary condition is set for the rotary kiln cylinder. The different inlet boundary conditions are shown in Tab. 6.

Table 6. Inlet Boundary Conditions

Type	Primary Air inlet	Pulverized coal with secondary air	Additional air inlet
Temperature	1200K	330K	330K
Flow rate	25m/s	2.5kg/s	5m/s

The temperature required in the simulation is generated with the combustion of pulverized coal, the specific composition and particle size are shown in Tab.7 and Tab.8. In the numerical simulation, the relevant parameters of the pulverized coal are consistent with the composition and particle size settings in the Tab. 7 and Tab. 8.

Table 7. Proximate analysis (as fired) and ultimate analysis (moisture ash free) of pulverized coal

Proximate Analysis				Ultimate Analysis					Low calorific value（MJ/kg）
F_{Cad}	V_{ad}	A_{ad}	M_{ad}	C_{ad}	H_{ad}	O_{ad}	N_{ad}	S_{ad}	24.09
47.75	29.00	20.3	2.92	62.35	3.66	31.97	0.90	1.12	

Where ad is air dry.

Table 8. Particle size distribution parameters of pulverized coal

Particle size type	Rosin-Rammler
Minimum particle size	1×10^{-6}m
Maximum particle size	2.8×10^{-4}m
Median particle size	6.1×10^{-5}m
Average particle size	7.2×10^{-5}m

4.5. Grid independence verification

This study investigates the impact of five different grid sizes on the simulation results while validating grid independence. The outlet temperature of the rotary kiln is considered a research parameter, with a pulverized coal injection rate of 2.5 kg/s. As the number of grid elements increases, the accuracy gradually improves, bringing the results closer to the actual temperature values, as shown in Fig. 8. When the number of grid elements exceeds 800k, the change in accuracy becomes relatively small. This study determined the grid elements of the model to be 800k, considering the computational load of the computer and the required accuracy, ensuring it remains within the acceptable range of engineering error. The minimum mesh quality for the 2×2×2 grid is 0.602, and the minimum angle is 29°, which meets the computational requirements.

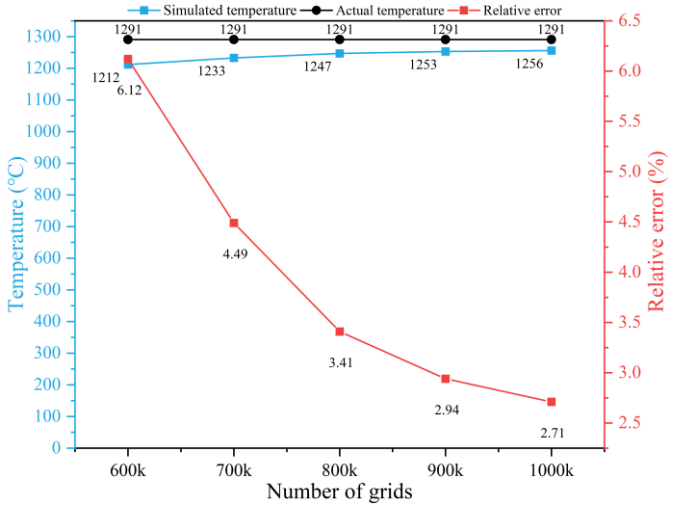

Fig. 8. Simulated and Actual Temperatures relative error

4.6. Model verification

The model used in this study is an improved version based on an actual rotary kiln in the plant. It is primarily applied to the generation of mullite and is mainly related to temperature. To validate the model, a comparison was performed using thermal calibration data from the on-site rotary kiln. The actual rotary kiln has a pulverized coal feed rate of 2.5 kg/s, and the model maintains consistency with this coal feed rate. Iterative calculations were performed using Fluent software, and the simulation was completed when the residual parameter curves converged and stabilized (with all residual values below 10^{-3}). By comparing the actual temperature data, the simulated outlet temperature of the rotary kiln was found to be 1247°C, while the actual measured temperature on site was 1291°C. This difference falls within a reasonable error range, meeting the requirements of this simulation.

Based on the validity of this model, this study compares the rotary kiln models of Gürtürk *et al.* [11], Huang *et al.* [13] and Wang *et al.* [22]. While there are minor differences in the burner design, the

main structure of the rotary kiln remains consistent. A temperature comparison was made with the models proposed by Huang *et al.* [13] and Wang *et al.* [22], as shown in the Tab. 9.

Table 9. Temperature comparison of different models

Type	Huang, Y.	Wang, G.	Modle in the study
Outlet temperature	1218℃-1354℃	1227℃-1327℃	1247℃

The outlet temperature of the model used in this study falls within the normal range. Moreover, the temperature variation trends observed in the numerical simulation results align with those of the other models, conforming to the fundamental principles of rotary kiln simulation.

4.7. Numerical Simulation Result and Discussion

In this paper, the numerical simulation is carried out without changing the inlet and outlet boundary conditions, and only the coal quantity is changed to find the minimum coal consumption to meet the production standards. With 2.5 kg/s as the benchmark, six pulverized coal flow rates (1.25 kg/s, 1.5 kg/s, 1.75 kg/s, 2.0 kg/s, 2.25 kg/s, and 2.5 kg/s) are selected. The simulation is completed when the equations of various parameters are run to convergence.

The distribution of the temperature field of the rotary kiln in the ZX section is shown in Fig. 9. The distribution of the CO_2 field in the ZX section is shown in Fig. 10.

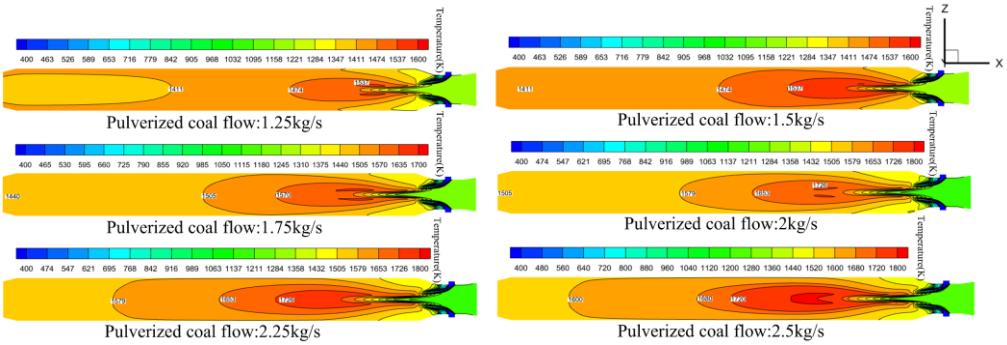

Fig. 9. Temperature Chart for Different Pulverized Coal Flow Rates

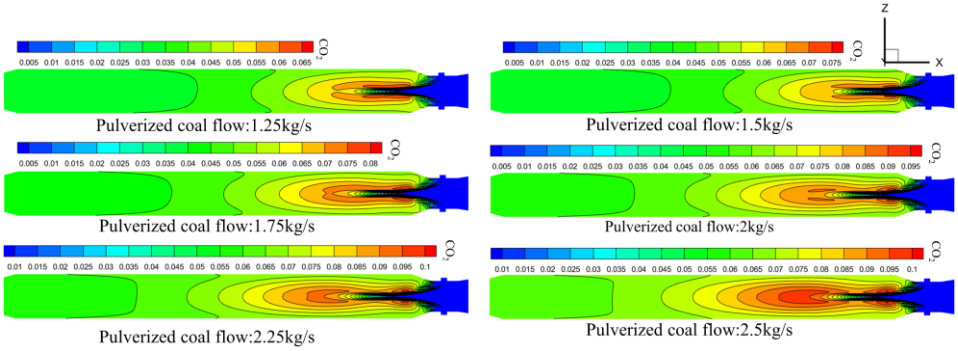

Fig. 10. CO_2 Chart for Different Pulverized Coal Flow Rates

As shown in Fig. 9, the pulverized coal starts to burn under the influence of hot air, and the temperature rises gradually with a large amount of pulverized coal burning to reach the highest temperature interval. The subsequent decrease in temperature is attributed to the burn-off of a large amount of pulverized coal. In contrast, the remaining small amount of pulverized coal and coke does not generate sufficient heat to maintain the high temperature. As a result, the temperature rises first, reaching the maximum temperature interval, and then gradually decreases. This temperature variation trend is consistent with previous oxy-coal combustion in a rotary cement kiln [23]. Meanwhile, the

reduction of the coal flow rate also leads to a gradual marginalization of the maximum temperature interval. Figure 10 shows that the CO_2 content is positively correlated with temperature, which means there is a high CO_2 content in the high-temperature region. In the study of oxygen concentration simulation in rotary kiln, coal combustion leads to an increase in both CO_2 concentration and temperature [24]. In this simulation, only the combustion of pulverized coal is considered, and CO_2 only comes from the combustion of pulverized coal.

The average and maximum temperatures in the rotary kiln are shown in Tab. 10. Due to large diameter and long cylinder of the rotary kiln, which results in a large effective volume, there is a large difference between the average and maximum temperatures in the kiln. In addition, variations in the amount of pulverized coal also cause temperature differences.

Table 10. Simulated Temperatures in Rotary Kiln

Amount of pulverized coal (kg/s)	1.25	1.50	1.75	2.00	2.25	2.50
Average temperature (℃)	1091	1159	1194	1260	1291	1321
Maximum temperature (℃)	1361	1428	1489	1586	1625	1660

The average temperature in the rotary kiln gradually decreases as the amount of pulverized coal decreases from 2.5 kg/s to 1.25 kg/s. The orthogonal test shows that mullite minerals containing 60% mullite can be produced when the particle size of coal kaolin is 4mm-8mm, and the residence time of materials is more than 1.5 h, the rotary kiln temperature reaches 1100℃. When the amount of pulverized coal is reduced to 1.5 kg/s, the average temperature of the rotary kiln reaches 1159℃.

Through numerical simulation analysis, the pulverized coal injection rate was reduced from 2.5 kg/s to 1.5 kg/s, which met the basic temperature requirements for production. For the production of mullite products, the pulverized coal usage only needs to reach 60% of the original amount to meet the production standards. This method significantly reduces energy consumption and prevents resource waste.

The distribution of the NO_X field in the ZX section is shown in Fig. 11.

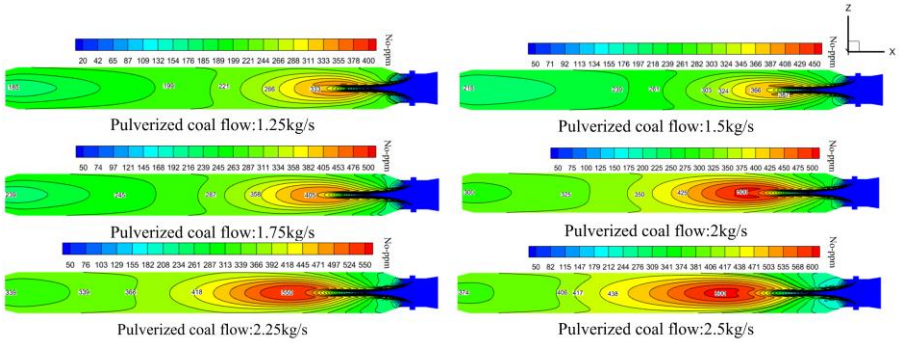

Fig. 11. NO_X Chart for Different Pulverized Coal Flow Rates

The NO_X-ppm for different amounts of pulverized coal showed a first increase, reaching the maximum concentration and then decreasing [22]. As the pulverized coal injection amount decreases, the concentration of NO_X gradually decreases as well. NO_X primarily originates from fuel combustion and thermal NO_X. A larger amount of pulverized coal combustion results in the production of more NO_X. Therefore, the trend of the NO_X distribution map is consistent with that of the temperature distribution map, with higher NO_X concentrations observed in areas of higher temperature.

Table 11. Simulated NO_X in Rotary Kiln

Amount of pulverized coal (kg/s)	1.25	1.50	1.75	2.00	2.25	2.50
Outlet NO_X-ppm	177	202	228	280	312	354

The reduction in pulverized coal injection leads to a corresponding decrease in the NO_X concentration at the outlet, with specific values shown in Tab 11. The NO_X concentration at the outlet complies with the national emission standard.

5. Conclusion

(1) Through scientific analysis of the orthogonal test, it is found that in the process of calcining coal kaolin in the rotary kiln, the highest percentage of mullite is 63.5%, 92.5%, and 93.4% when the temperature reaches 1100℃, 1300℃, and 1500℃, respectively. The range analysis shows that the best effect is obtained under the conditions of 4mm-8mm particle size, 1500℃ temperature, and 1.5h residence time. The analysis of variance result shows that the main factors affecting the mullite content, in order of importance, are rotary kiln temperature, particle size of coal kaolin, and residence time of materials.

(2) The experimental results indicate an optimal temperature of 1100℃, which meets the basic production requirements. Through numerical simulation, the pulverized coal injection rate was reduced to 1.5 kg/s. Under this condition, the average temperature in the kiln is 1159℃. The use of pulverized coal is reduced by 40%. As a primary fuel in industrial production, adjusting the amount of pulverized coal according to the specific needs of different products has a positive impact on both the environment and energy efficiency. The result provides a reference for subsequent production operations and technical improvements.

(3) Secondary air temperature, as an important parameter in rotary kiln operation, has a significant impact on the kiln temperature. In future research, secondary air temperature can be used as a starting point to explore its effect on the temperature profile within the kiln. The rotary kiln can also achieve energy savings and carbon reduction by replacing pulverized coal with alternative fuels (petroleum coke and biomass fuels).

References

[1] Liu, Y., *et al*., Assessment of pozzolanic activity of calcined coal-series kaolin, *Applied Clay Science*, 143 (2017), pp. 159-167

[2] Bu, X., *et al*., Removal of fine quartz from coal-series kaolin by flotation, *Applied Clay Science*, 143 (2017), pp. 437-444

[3] Xu, X., *et al*., Microstructural evolution, phase transformation, and variations in physical properties of coal series kaolin powder compact during firing, *Applied Clay Science*, 115 (2015), pp. 76-86

[4] Ptáček, P., *et al*., The kinetics of Al–Si spinel phase crystallization from calcined kaolin, *Journal of Solid State Chemistry*, 183 (2010), 11, pp. 2565-2569

[5] Ondro, T., *et al*., Kinetic analysis of sinter-crystallization of mullite and cristobalite from kaolinite, *Thermochimica Acta*, 678 (2019), p. 178312

[6] Yuan, S., *et al*., Effects of carbonaceous matter additives on kinetics, phase and structure evolution of coal-series kaolin during calcination, *Applied Clay Science*, 165 (2018), pp. 124-134

[7] Chargui, F., *et al*., Mullite fabrication from natural kaolin and aluminium slag, *Boletín De La Sociedad Española De Cerámica Y Vidrio*, 57 (2018), 4, pp. 169-177

[8] Chen, C., Tuan, W., Evolution of Mullite Texture on Firing Tape-Cast Kaolin Bodies, *Journal of the American Ceramic Society*, 85 (2002), 5, pp. 1121-1126

[9] Liu, X. Y., Specht, E., Mean residence time and hold-up of solids in rotary kilns, *Chemical Engineering Science*, 61 (2006), 15, pp. 5176-5181

[10] Bojanovský, J., *et al*., Rotary Kiln, a Unit on the Border of the Process and Energy Industry—Current State and Perspectives, *Sustainability*, 14 (2022), 21, p. 13903

[11] Gürtürk, M., *et al*., CFD analysis of a rotary kiln using for plaster production and discussion of the effects of flue gas recirculation application, *Heat and Mass Transfer*, 54 (2018), 10, pp. 2935-2950

[12] Ariyaratne, W. K. H., *et al*., CFD modelling of meat and bone meal combustion in a cement rotary kiln – Investigation of fuel particle size and fuel feeding position impacts, *Chemical Engineering Science*, 123 (2015), pp. 596-608

[13] Huang, Y., *et al*., Numerical simulation of pulverized coal combustion in rotary kilns with different oxygen concentrations, *Energy Sources. Part a, Recovery, Utilization, and Environmental Effects*, 44 (2022), 2, pp. 4510-4524

[14] Xia, S., *et al*., The application of orthogonal test method in the parameters optimization of PEMFC under steady working condition, *International Journal of Hydrogen Energy*, 41 (2016), 26, pp. 11380-11390

[15] Vuthaluru, R., Vuthaluru, H. B., Modelling of a wall fired furnace for different operating conditions using FLUENT, *Fuel Processing Technology*, 87 (2006), 7, pp. 633-639

[16] Xu, J., et al., A Soft Sensor Modeling of Cement Rotary Kiln Temperature Field Based on Model-Driven and Data-Driven Methods, Ieee Sensors Journal, 21 (2021), 24, pp. 27632-27639

[17] Cecílio, D. M., *et al*., Industrial Rotary Kiln Burner Performance with 3D CFD Modeling, *Fuels*, 4 (2023), 4, pp. 454-468

[18] Rahman, A., *et al*., Recent development on the uses of alternative fuels in cement manufacturing process, *Fuel (Guildford)*, 145 (2015), pp. 84-99

[19] Bäckström, D., *et al*., On the use of alternative fuels in rotary kiln burners — An experimental and modelling study of the effect on the radiative heat transfer conditions, *Fuel Processing Technology*, 138 (2015), pp. 210-220

[20] Kobayashi, H., *et al*., Coal devolatilization at high temperatures, *Symposium (International) On Combustion*, 16 (1977), 1, pp. 411-425

[21] Wang, B., Kao, H., Numerical simulation of O_2/CO_2 combustion in decomposition furnace, *Thermal Science*, 27 (2023), 5 Part B, pp. 4307-4320

[22] Wang, G., et al., Numerical simulation of pulverized coal combustion in a rotary kiln under O_2/CO_2 atmosphere, *Thermal Science*, 27 (2023), 6 Part B, pp. 4935-4945

[23] Wang, M., et al., Numerical simulation of oxy-coal combustion in a rotary cement kiln, *Applied Thermal Engineering*, 103 (2016), pp. 491-500

[24] Cecílio, D. M., et al., Industrial Rotary Kiln Burner Performance with 3D CFD Modeling, *Fuels*, 4 (2023), 4, pp. 454-468

Submitted: 19.10.2024.
Revised: 23.12.2024
Accepted: 27.12.2024.